Supplementary material for The emergence of a new wintertime Arctic energy balance regime

O. Miyawaki[1], T. A. Shaw[2], M. F. Jansen[2]

[1]Climate and Global Dynamics Laboratory, National Center for Atmospheric Research
[2]Department of the Geophysical Sciences, The University of Chicago

Corresponding author: Osamu Miyawaki, `miyawaki@ucar.edu`

1 Response in individual CMIP6 and CMIP5 models

The RAE to RCAE regime transition occurs in 9 out of 10 CMIP6 models analyzed here (black lines in Fig. S1). Among models that exhibit the wintertime regime transition, sea ice melts, the surface inversion vanishes, and convective precipitation emerges (purple and blue lines in Fig. S3 and S4). CMIP5 models also exhibit the link between the time-dependent response of energy balance regimes and the surface inversion and convective precipitation fraction (Fig. S22 and S23). The exception is IPSL-CM5A-LR, where convective precipitation remains 0 despite undergoing the RAE to RCAE regime transition (Fig. S23i).

9 out of 10 CMIP6 models exhibit the two distinct phases of the regime transition (gray and red lines in Fig. S5). 6 of the 9 CMIP5 models exhibit the two phases of the regime transition (Fig. S25). The exceptions are HadGEM2-ES, where reduced advective heating dominates the full R_1 response, and GISS-E2-R and IPSL-CM5A-LR, where enhanced radiative cooling dominates the full response.

The clear-sky longwave cooling response to anthropogenic forcing contributes to the enhanced radiative cooling response in all CMIP6 (red lines in Fig. S6) and CMIP5 models (Fig. S26). The contribution of the cloudy-sky longwave cooling response varies among models. For example, the cloudy-sky contribution is close to 0 in CESM2-WACCM, MIROC-ES2L, CSIRO-Mk3-6-0, GISS-E2-H, and GISS-E2-R whereas the cloudy-sky contribution is equally or more important than the clear-sky contribution in GISS-E2-1-G, CCSM4, and IPSL-CM5A-LR. The cloudy-sky contribution in several CMIP6 models is time dependent, where the cloudy-sky contribution is largest during the regime transition and weakens thereafter as the Arctic approaches equilibrium.

RRTMG captures the clear-sky longwave cooling response for most CMIP6 (compare black and red lines in Fig. S6) and CMIP5 models (Fig. S26). The exceptions are CanESM5, GISS-E2-1-H, GISS-E2-H, and GISS-E2-R where RRTMG overpredicts the radiative cooling response and CSIRO-Mk3-6-0 where RRTMG underpredicts the response. The enhanced greenhouse effect from warming and the moistening associated with fixed relative humidity explains the clear-sky response in all CMIP6 (orange lines in Fig. S7) and CMIP5 models (orange lines in Fig. S27).

2 Deriving the Q flux to capture the thermodynamic effect of sea ice

The goal of imposing the Q flux in AQUAnomelt is to capture the climatology of AQUAmelt in the absence of an interactive sea-ice module. To derive the Q flux (Q) that mimics the thermodynamic effect of sea ice, consider the surface energy budget for AQUAnomelt:

$$C^{nm}\frac{\partial T_s^{nm}}{\partial t} + Q = SW^{nm} + LW^{nm} + LH^{nm} + SH^{nm} = F_{SFC}^{nm}\,, \tag{1}$$

and for AQUAmelt:

$$C^{m}\frac{\partial T_s^{m}}{\partial t} + F_{melt}^{m} + F_{cond}^{m} = SW^{m} + LW^{m} + LH^{m} + SH^{m} = F_{SFC}^{m}\,, \tag{2}$$

where F_{SFC} is the net surface energy flux, F_{melt} is the energy flux associated with surface melting of snow or sea ice, F_{cond} is conductive flux through snow and sea ice, SW is the net surface shortwave flux, LW is the net surface longwave flux, LH is surface latent heat flux, SH is surface sensible heat flux, T_s is the surface temperature, and C is the surface heat capacity. The superscripts nm and m indicate the value is associated with AQUAnomelt and AQUAmelt, respectively.

Subtracting equation (2) from (1), we obtain:

$$\begin{aligned} Q =& C^{m}\frac{\partial T_s^{m}}{\partial t} + F_{melt}^{m} + F_{cond}^{m} - C^{nm}\frac{\partial T_s^{nm}}{\partial t} + \\ & SW^{nm} - SW^{m} + LW^{nm} - LW^{m} + LH^{nm} - LH^{m} + SH^{nm} - SH^{m}\,. \end{aligned} \tag{3}$$

Table S1. List of the 10 CMIP6 and 9 CMIP5 models that are used for the multimodel mean of the extended SSP585 and RCP8.5 runs. The ensemble member used is in parenthesis.

CMIP6	CMIP5
ACCESS-CM2 (r1i1p1f1)	bcc-csm1-1 (r1i1p1)
ACCESS-ESM1-5 (r1i1p1f1)	CCSM4 (r1i1p1)
CanESM5 (r1i1p1f1)	CNRM-CM5 (r1i1p1)
CESM2-WACCM (r1i1p1f1)	CSIRO-Mk3-6-0 (r1i1p1)
GISS-E2-1-G (r3i1p1f2)	GISS-E2-H (r1i1p1)
GISS-E2-1-H (r3i1p1f2)	GISS-E2-R (r1i1p1)
IPSL-CM6A-LR (r1i1p1f1)	HadGEM2-ES (r1i1p1)
MIROC-ES2L (r1i1p1f2)	IPSL-CM5A-LR (r1i1p1)
MRI-ESM2-0 (r1i1p1f1)	MPI-ESM-LR (r1i1p1)
UKESM1-0-LL (r4i1p1f2)	

All quantities with a superscript nm are unknown because they emerge only after running the model with the imposed Q. To close this problem, we first require that the sum of the following terms in AQUAnomelt matches that of AQUAmelt:

$$C^{nm}\frac{\partial T_s^{nm}}{\partial t} + LW^{nm} + LH^{nm} + SH^{nm} = C^{nm}\frac{\partial T_s^{m}}{\partial t} + LW^{m} + LH^{m} + SH^{m} \tag{4}$$

Substituting equation (4) into (3),

$$Q = \underbrace{F_{SFC}^m - C^{nm}\frac{\partial T_s^m}{\partial t}}_{\text{surface heat capacity effect, } Q_C} + \underbrace{SW^{nm} - SW^m}_{\text{shortwave effect, } Q_{SW}} . \tag{5}$$

Q is composed of two distinct thermodynamic effects of sea ice. First, the smaller surface heat capacity of sea ice and the presence of melt and conductive fluxes amplify the seasonal cycle of surface temperature. Second, the higher surface albedo of sea ice compared to open ocean acts to cool the surface temperature year round. The surface heat capacity effect, Q_C, can be computed directly from the diagnosed surface heat fluxes and surface temperature in AQUAmelt. The shortwave effect, Q_{SW}, is estimated using an analytic radiative transfer model (Winton, 2005). Substituting equation (19) in Winton (2005) for SW^{nm} and simplifying yields the following expression for the shortwave effect of sea ice:

$$Q_{SW} = \frac{SW_\downarrow^m}{1 - \alpha_S^{nm}\alpha_\uparrow^m}(\alpha_S^m - \alpha_S^{nm})(1 - \alpha_\uparrow^m)\,, \tag{6}$$

where $SW_\downarrow^m$ is the downward surface shortwave flux in AQUAmelt, α_S is the surface albedo where $\alpha_S^{nm} = 0.07$ for open ocean and α_S^m is the diagnosed surface albedo in AQUAmelt, and $\alpha_\uparrow$ is the atmospheric shortwave reflectivity to upwelling fluxes. $\alpha_\uparrow^m$ is computed for AQUAmelt following equation (18) in Winton (2005):

$$\alpha_\uparrow^m = 0.05 + 0.85\left(1 - \frac{SW_\downarrow^m}{SW_{\downarrow,clear}^m}\right), \tag{7}$$

where $SW_{\downarrow,clear}^m$ is the clear-sky downward surface shortwave flux in AQUAmelt.

AQUAnomelt captures the climatology of the AQUAmelt surface temperature for both the seasonal cycle and the annual mean (compare purple and blue lines in Fig. S9). Furthermore, the vertical structure of the Arctic temperature profile in AQUAnomelt is consistent with the AQUAmelt climatology (Fig. S10).

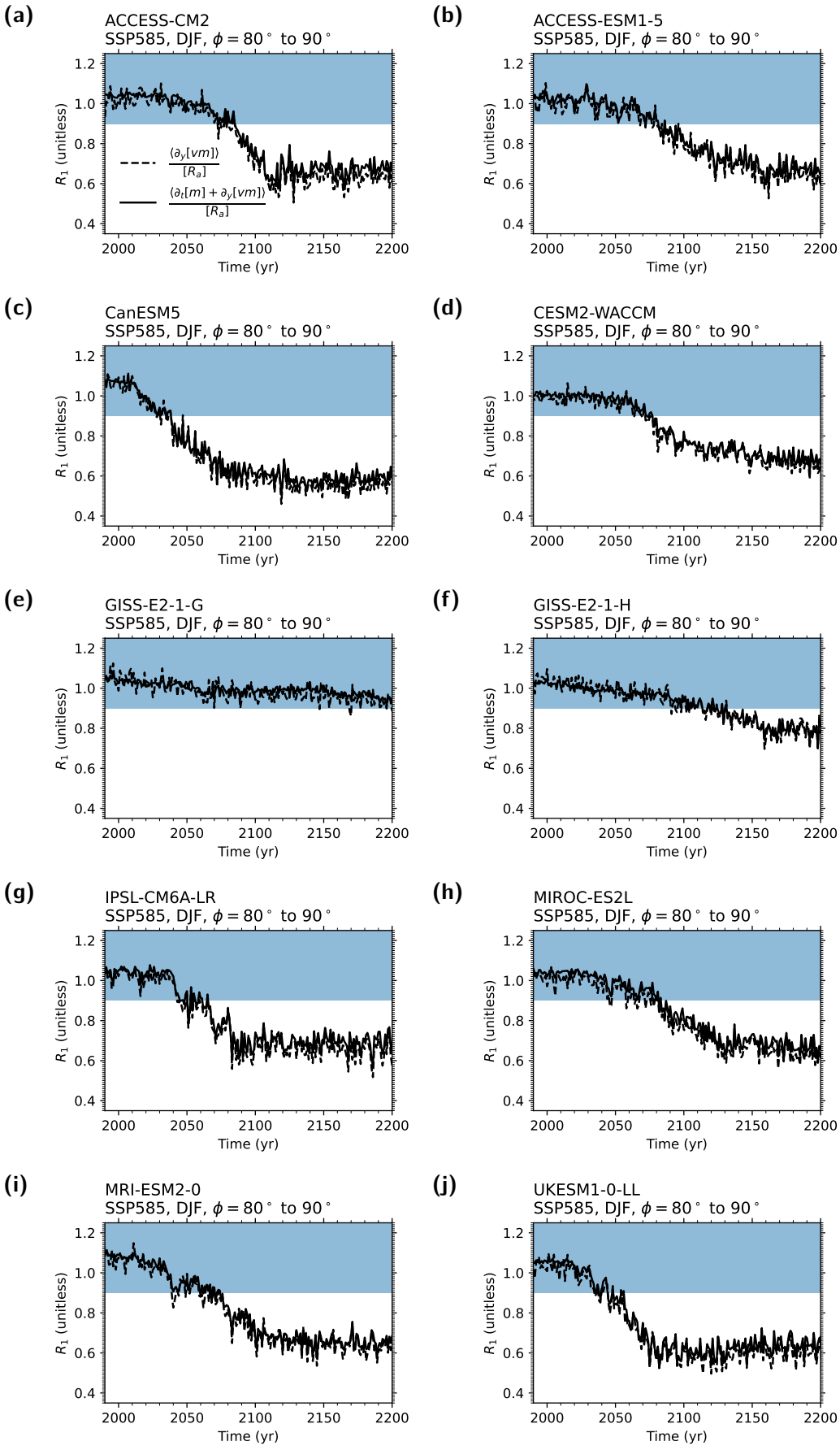

Figure S1. The wintertime (DJF) energy balance regime quantified using $R_1 = \langle \partial_t[m] + \partial_y[vm] \rangle / [R_a]$ (solid black, see equation (1) in the main text) and an alternative definition without the storage term, $\langle \partial_y[vm] \rangle / [R_a]$ (dashed black), for individual CMIP6 models of the extended SSP585 run. Blue and white regions indicate RAE and RCAE, respectively.

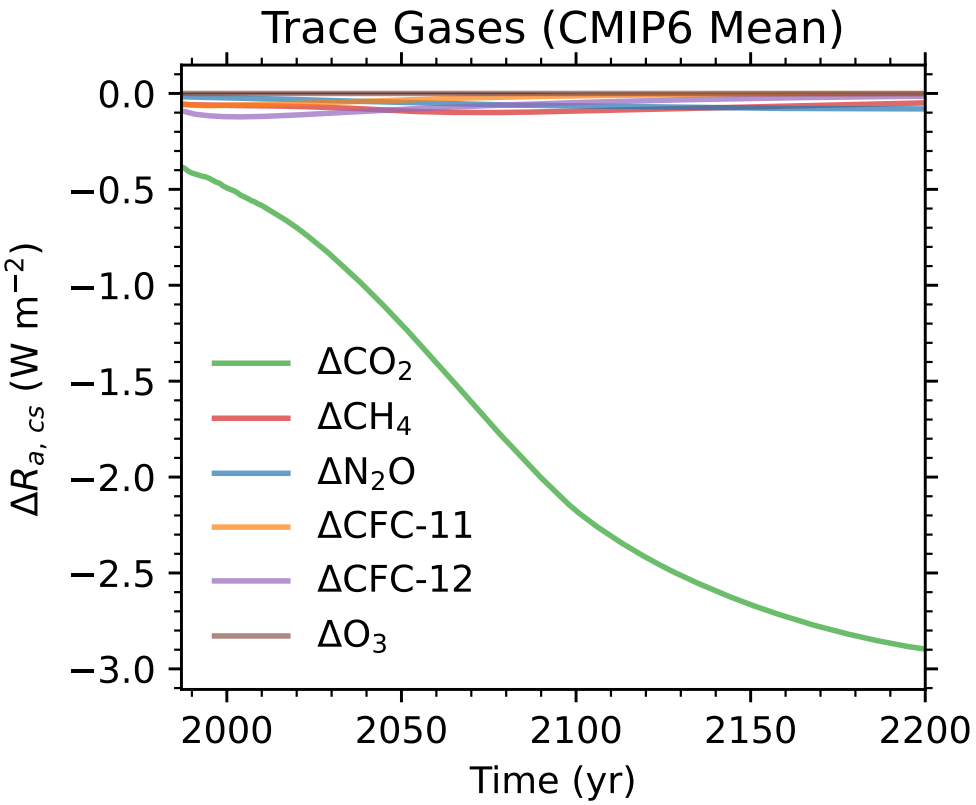

Figure S2. The contribution of carbon dioxide (green), methane (red), nitrous oxide (blue), trichlorofluoromethane (orange), dichlorodifluoromethane (purple), and ozone (brown) on the wintertime (DJF) clear-sky radiative cooling response (gray) is decomposed using RRTMG.

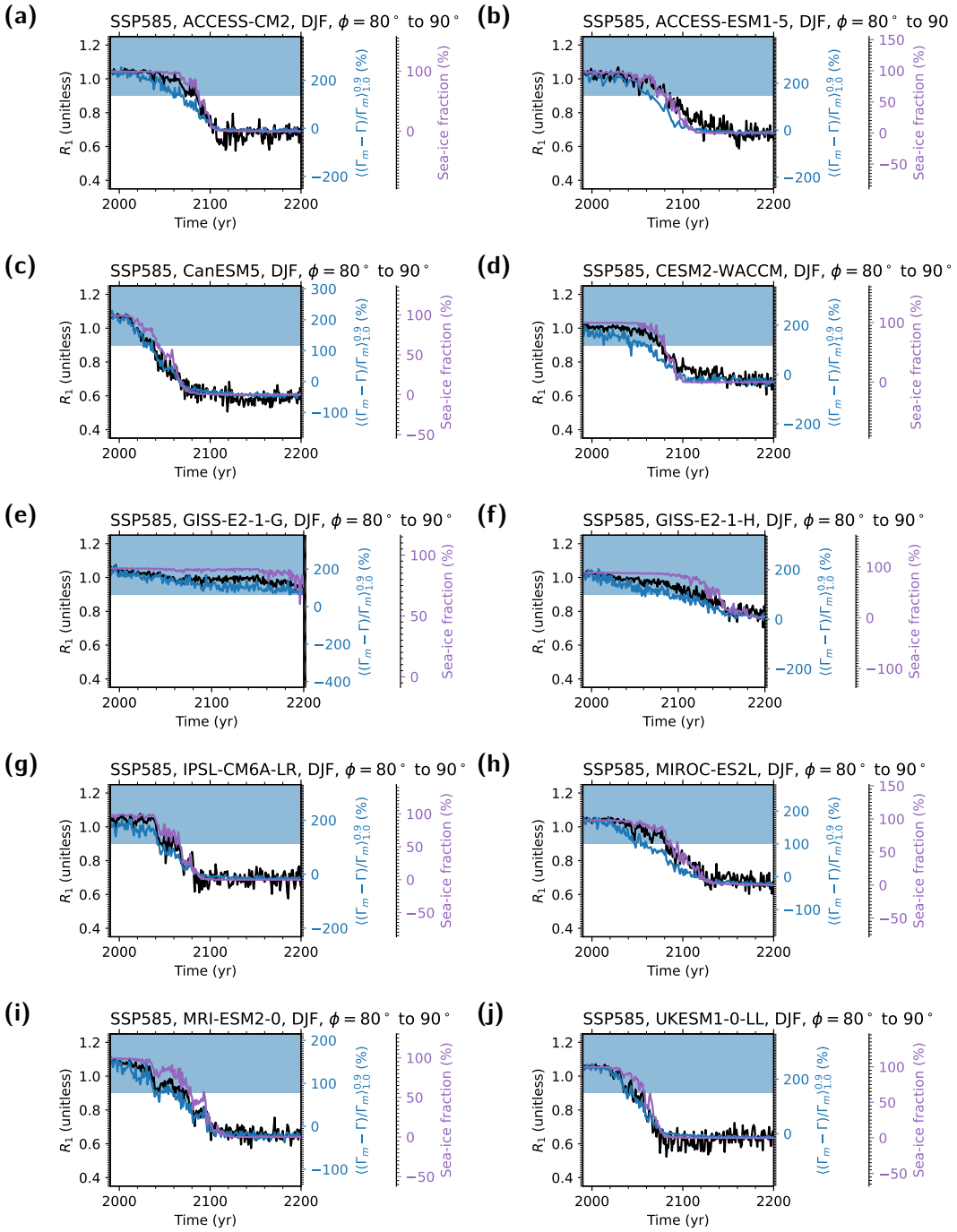

Figure S3. Same as Fig. 1a but (a–j) for individual CMIP6 models.

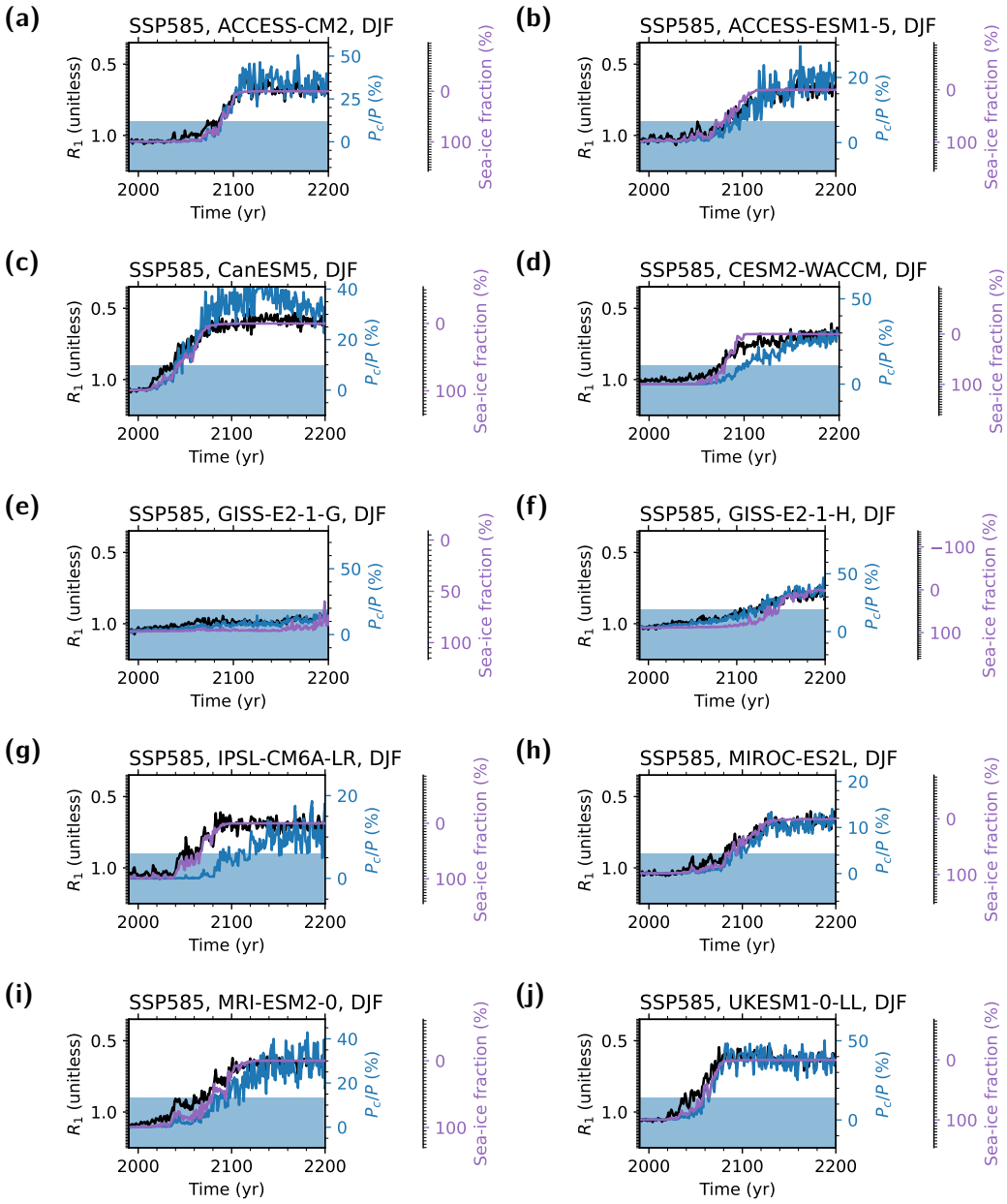

Figure S4. Same as Fig. 1b but (a–j) for individual CMIP6 models.

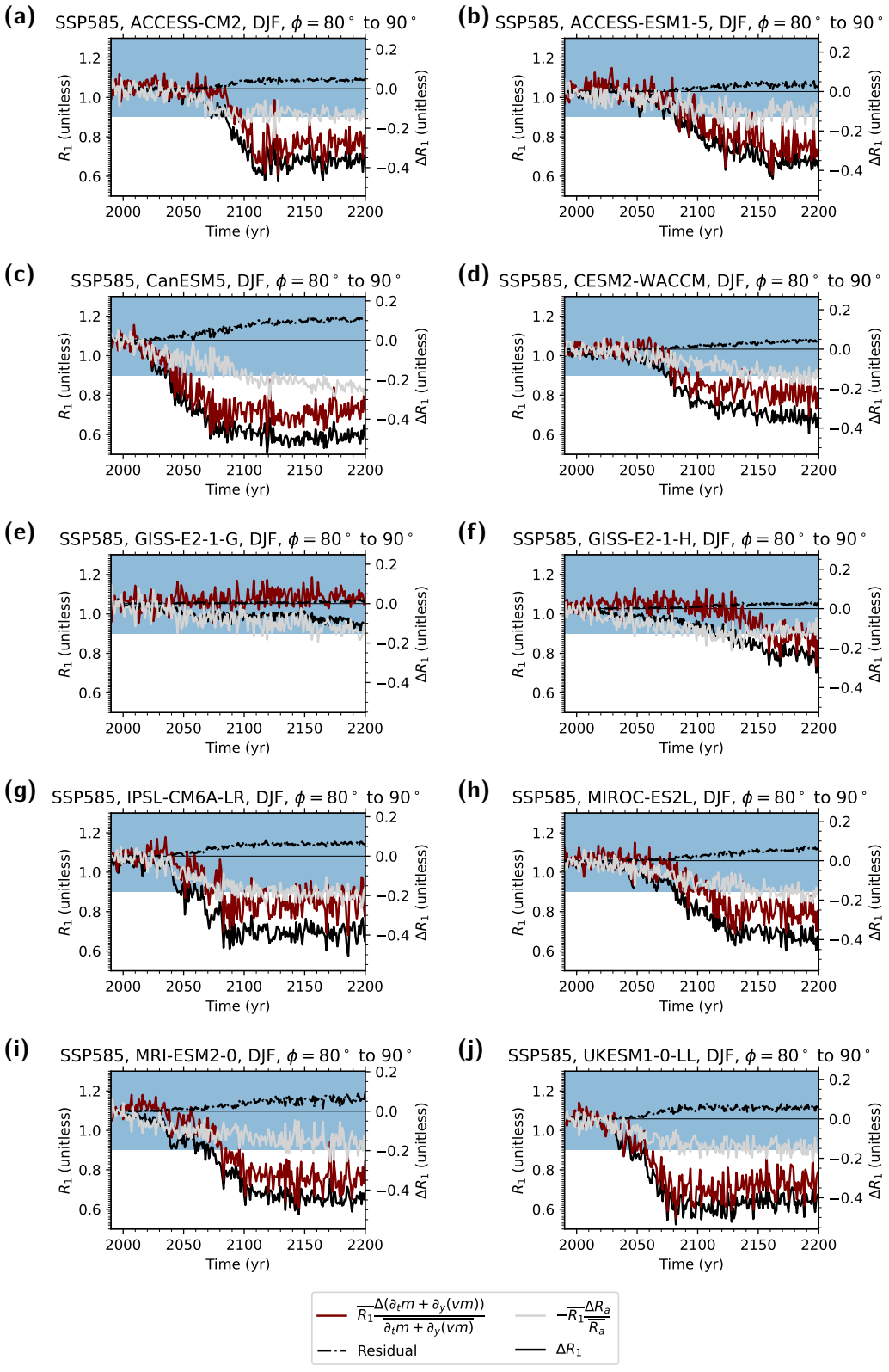

Figure S5. Same as Fig. 2 but (a–j) for individual CMIP6 models.

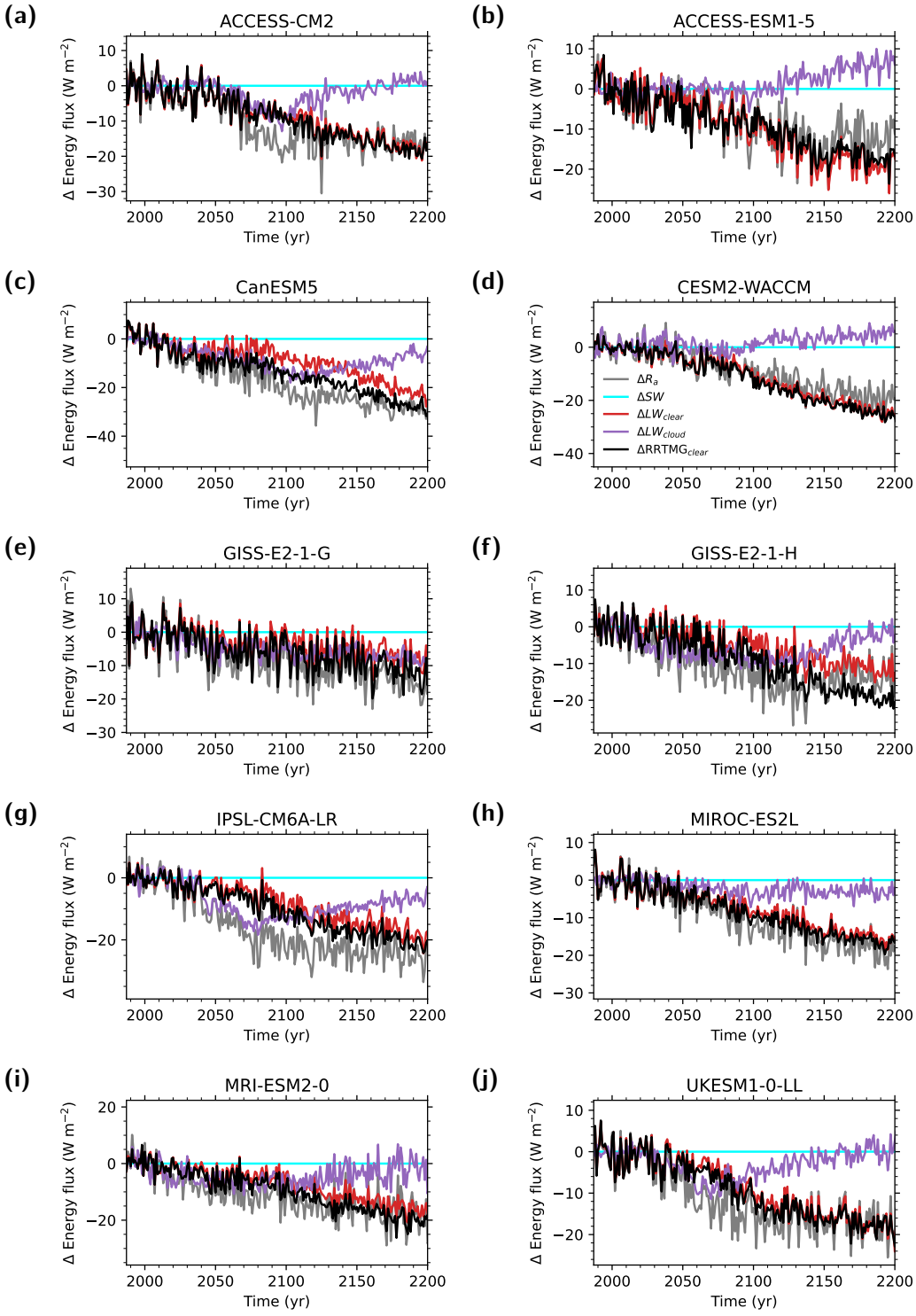

Figure S6. Same as Fig. 3a but (a–j) for individual CMIP6 models.

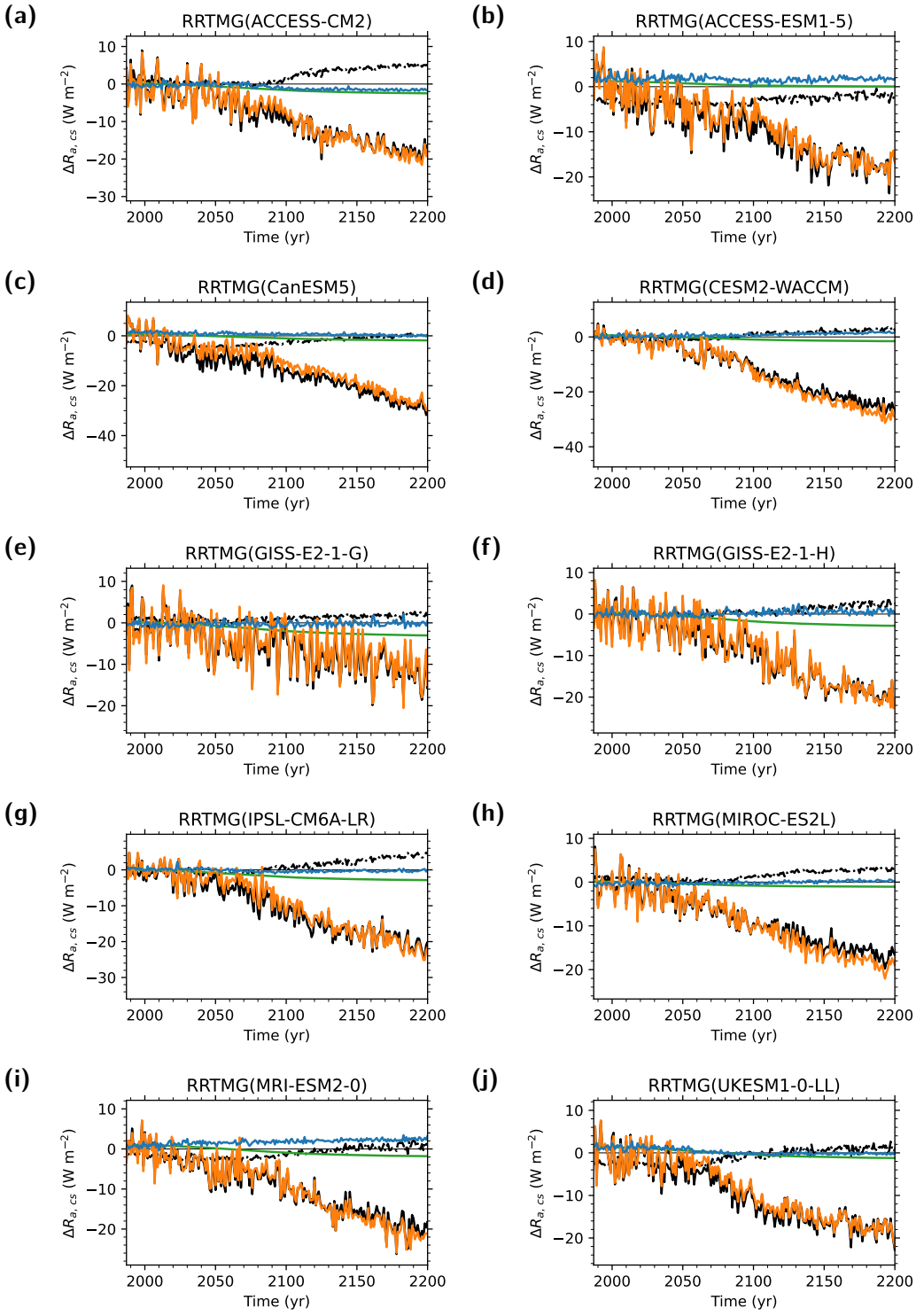

Figure S7. Same as Fig. 3b but (a–j) for individual CMIP6 models.

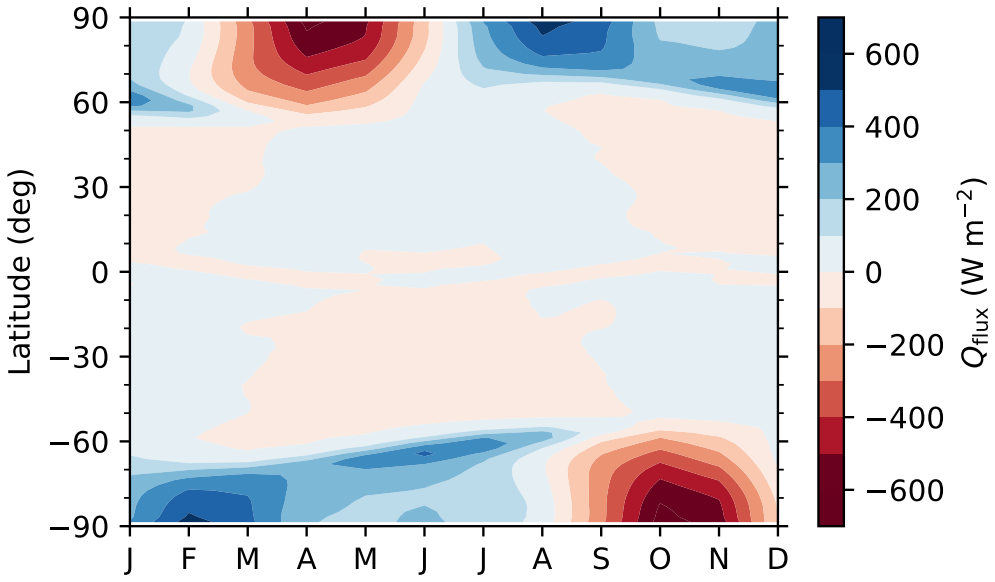

Figure S8. The latitudinal and seasonal structure of the imposed Q flux in AQUAnomelt. Positive values correspond to heat flux divergence, a cooling influence on the surface energy budget.

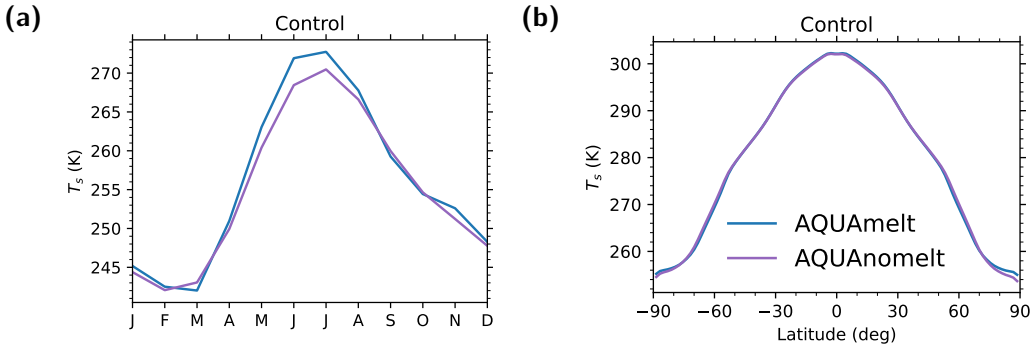

Figure S9. (a) The seasonal cycle of Arctic surface temperature and (b) the latitudinal structure of annual mean surface temperature for the AQUAmelt (blue) and AQUAnomelt (purple) historical-run climatology. The climatology is the average the last 20 years of each run.

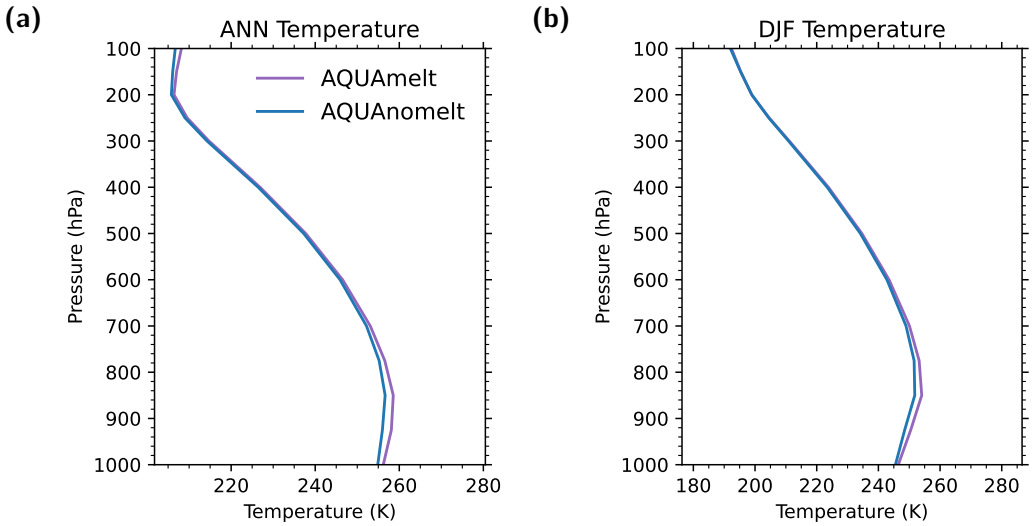

Figure S10. (a) Annual mean (ANN) and (b) wintertime (DJF) Arctic vertical temperature profile for the AQUAmelt (blue) and AQUAnomelt (purple) historical-run climatology. The climatology is the average the last 20 years of each run.

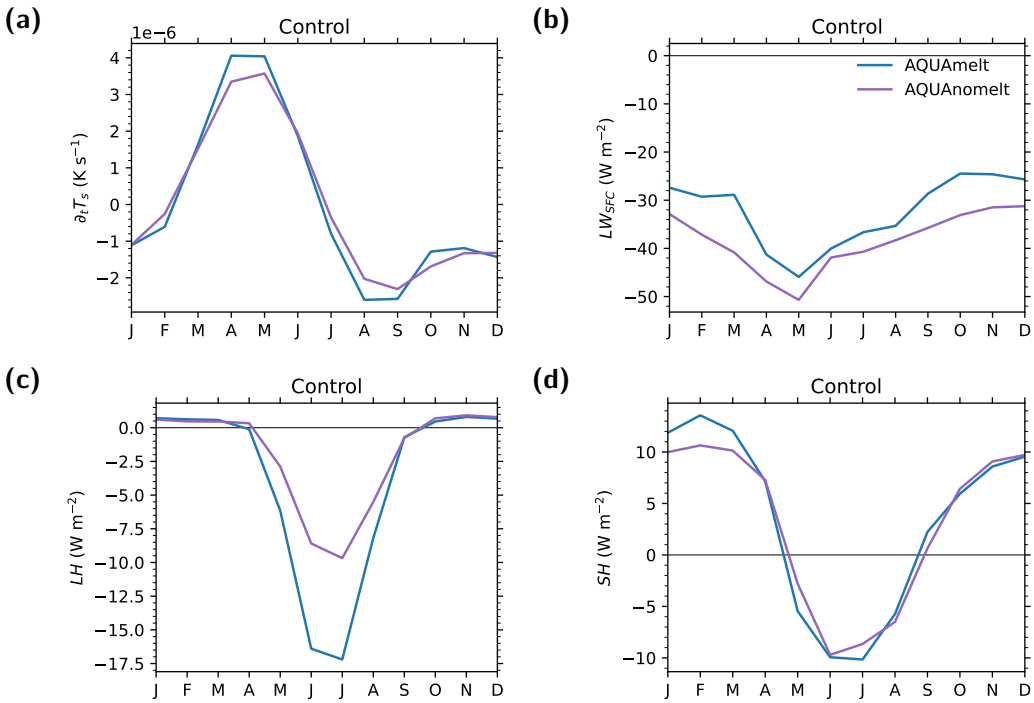

Figure S11. The seasonal cycle of Arctic (a) surface temperature tendency, (b) surface longwave radiative flux, (c) surface latent heat flux, and (d) surface sensible heat flux for the AQUAmelt (blue) and AQUAnomelt (purple) historical-run climatology. The climatology is the average the last 20 years of each run.

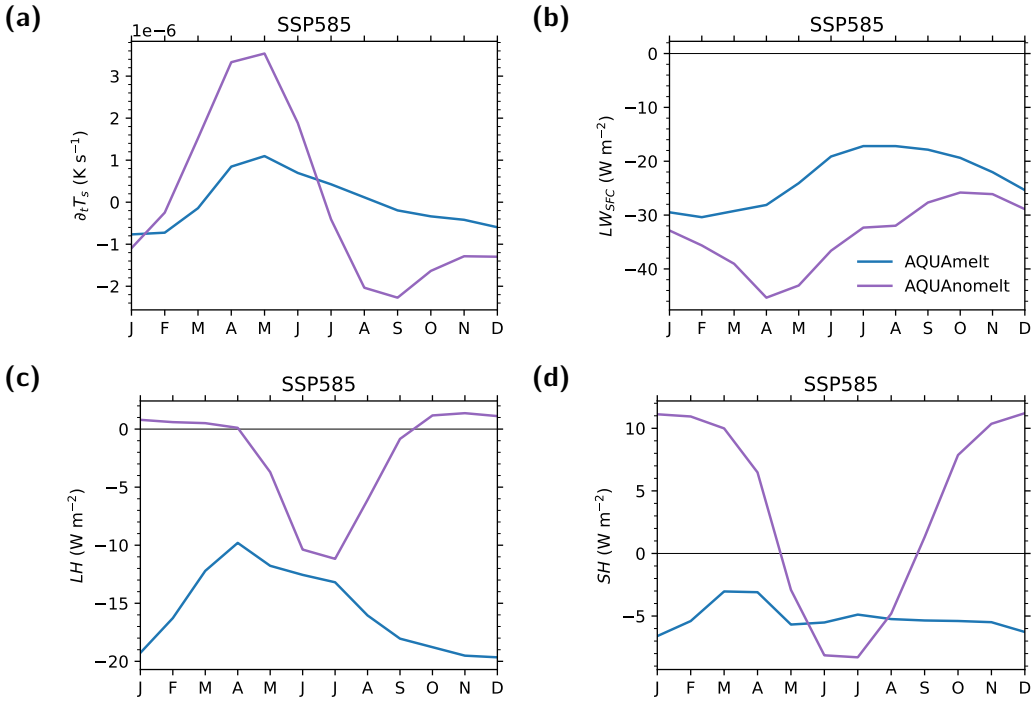

Figure S12. Same as Fig. S11 but for the SSP585 run climatology. The climatology is the average the last 20 years of each run (i.e., 2180–2200).

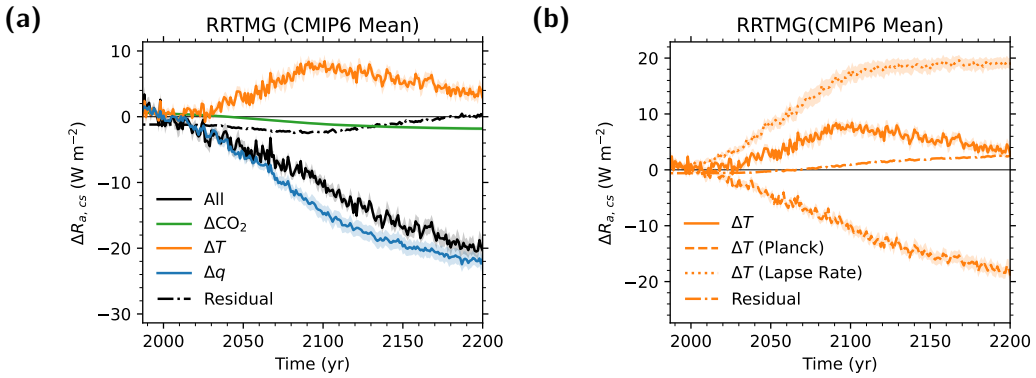

Figure S13. (a) Similar to Fig. 3b but showing an alternative decomposition that separates the contribution of warming at fixed specific humidity (i.e. holding CO_2 and specific humidity fixed, orange line) and moistening (i.e. holding CO_2 and temperature fixed, blue line). (b) The warming contribution in the absence of moistening is further decomposed into contributions from vertically uniform warming (Planck effect, dashed orange) and deviations therefrom (lapse rate effect, dotted orange).

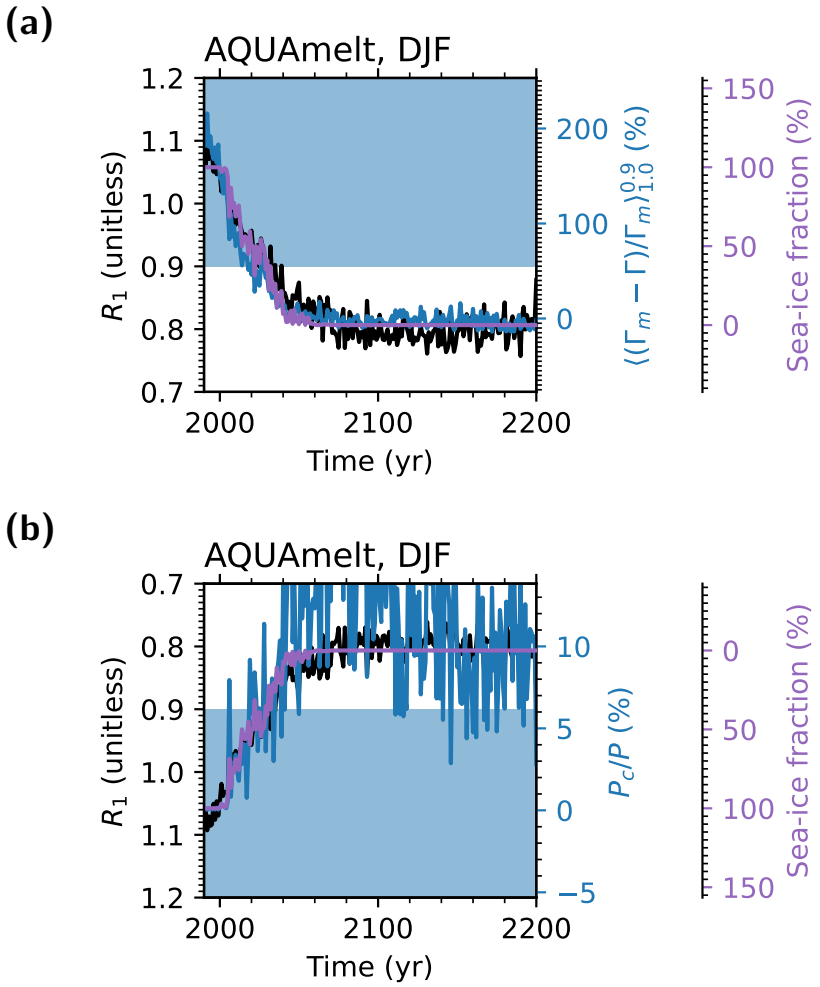

Figure S14. Same as Fig. 1 but for AQUAmelt.

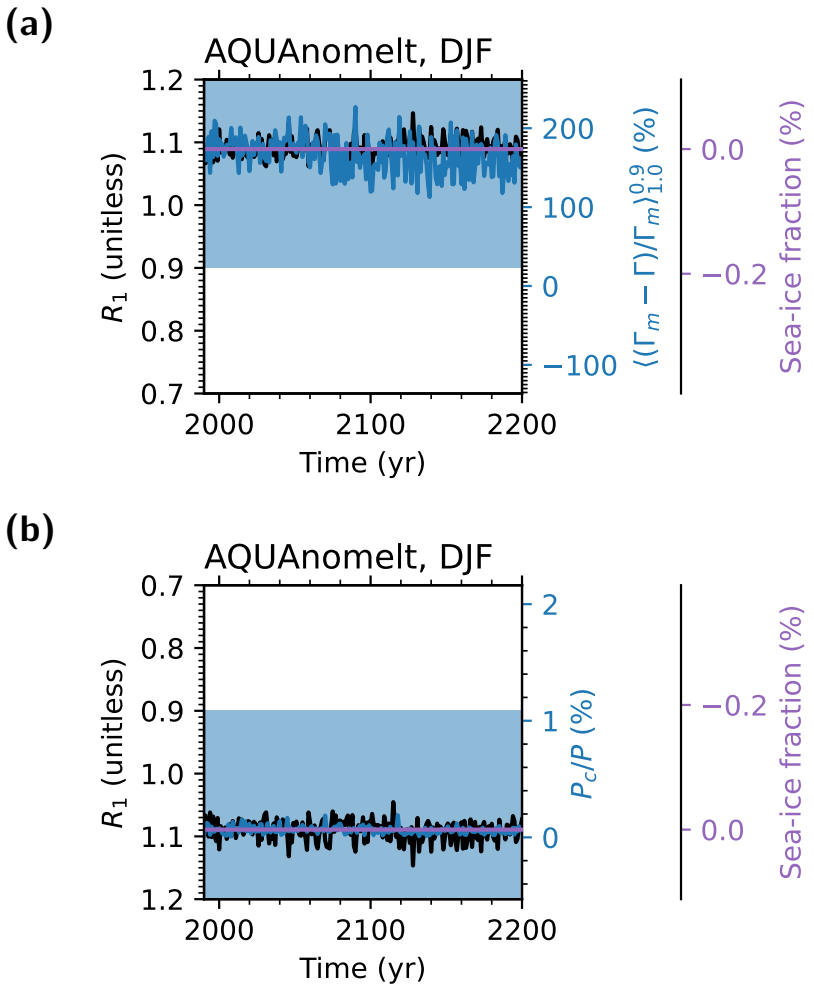

Figure S15. Same as Fig. 1 but for AQUAnomelt.

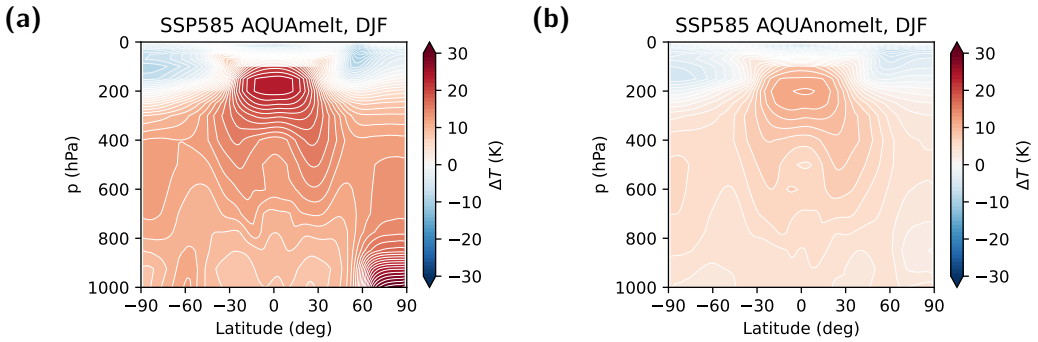

Figure S16. (a) The latitudinal and vertical warming response for the Northern Hemisphere winter season (DJF) for (a) AQUAmelt and (b) AQUAnomelt. The warming response is computed as the difference between the temperature averaged over year 2180 to 2200 of the SSP585 run and the last 20 years of the historical run. The contour interval is 1 K. Note that the climate is hemispherically symmetric in the aquaplanets: the asymmetry shown here is a seasonal asymmetry (surface-amplified polar warming is weak in the summer hemisphere).

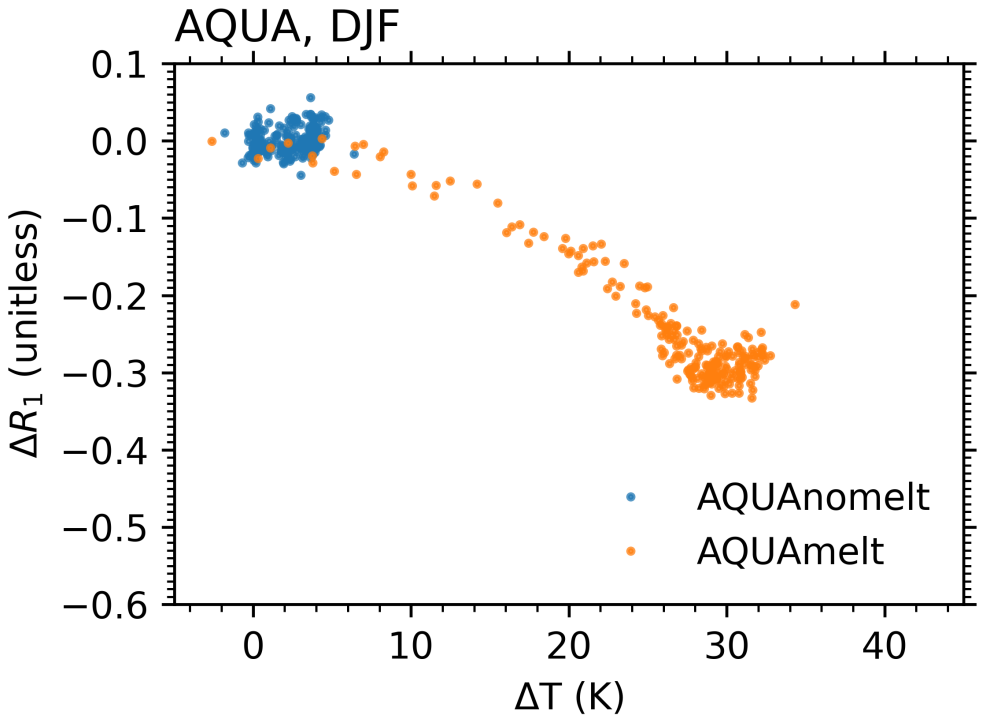

Figure S17. Wintertime ΔR_1 versus ΔT (2 m warming) for AQUAnomelt (blue) and AQUAmelt (black). Each dot is one DJF seasonal mean.

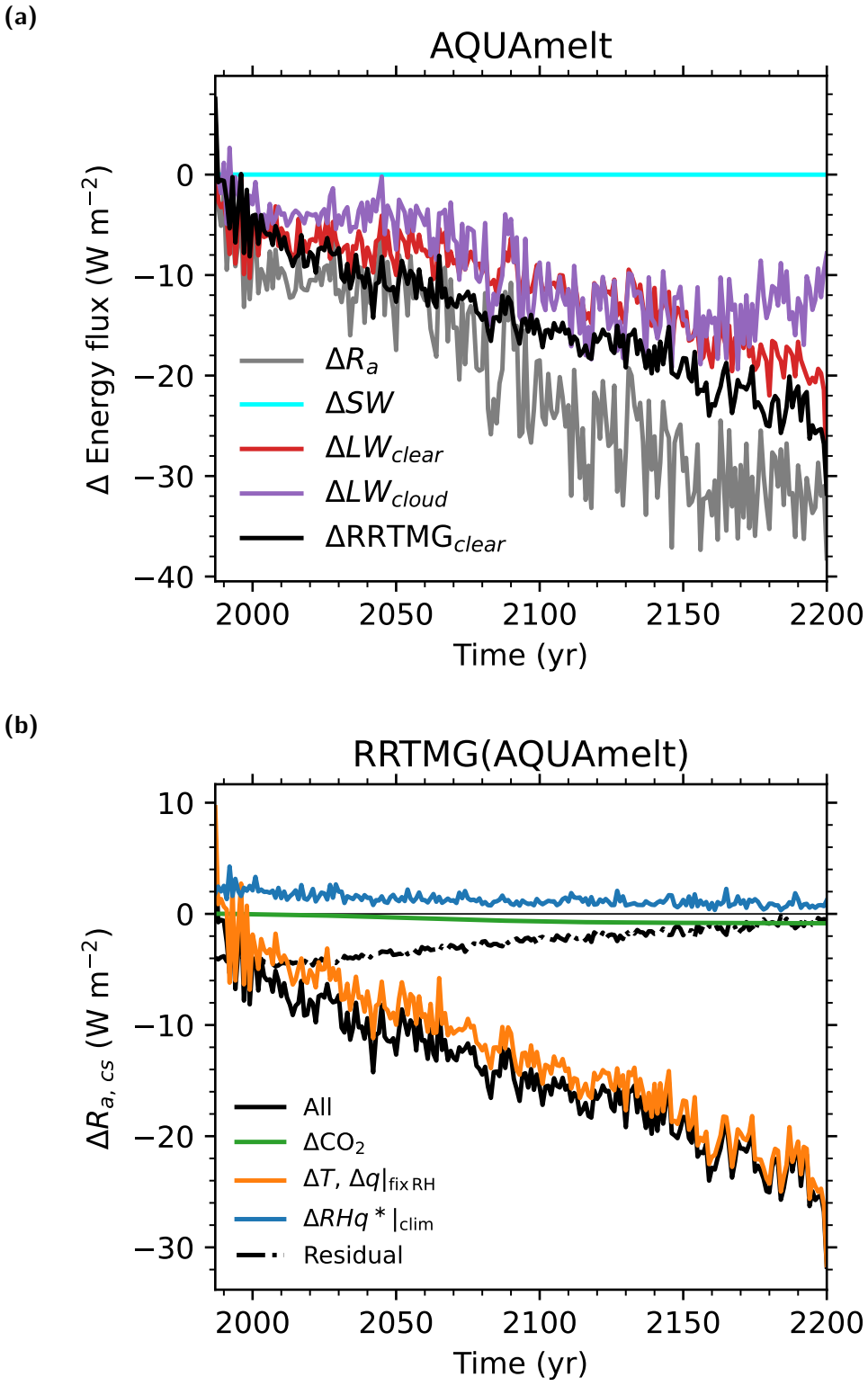

Figure S18. Same as Fig. 3 but for AQUAmelt.

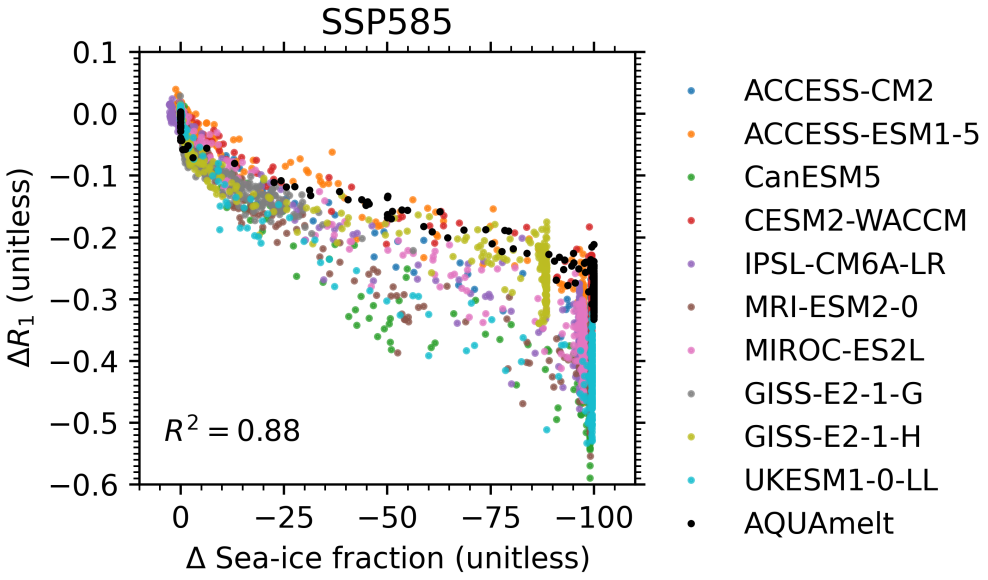

Figure S19. Wintertime ΔR_1 versus Δ sea-ice fraction for CMIP6 models (colors) and AQUAmelt (black). Each dot is one DJF seasonal mean.

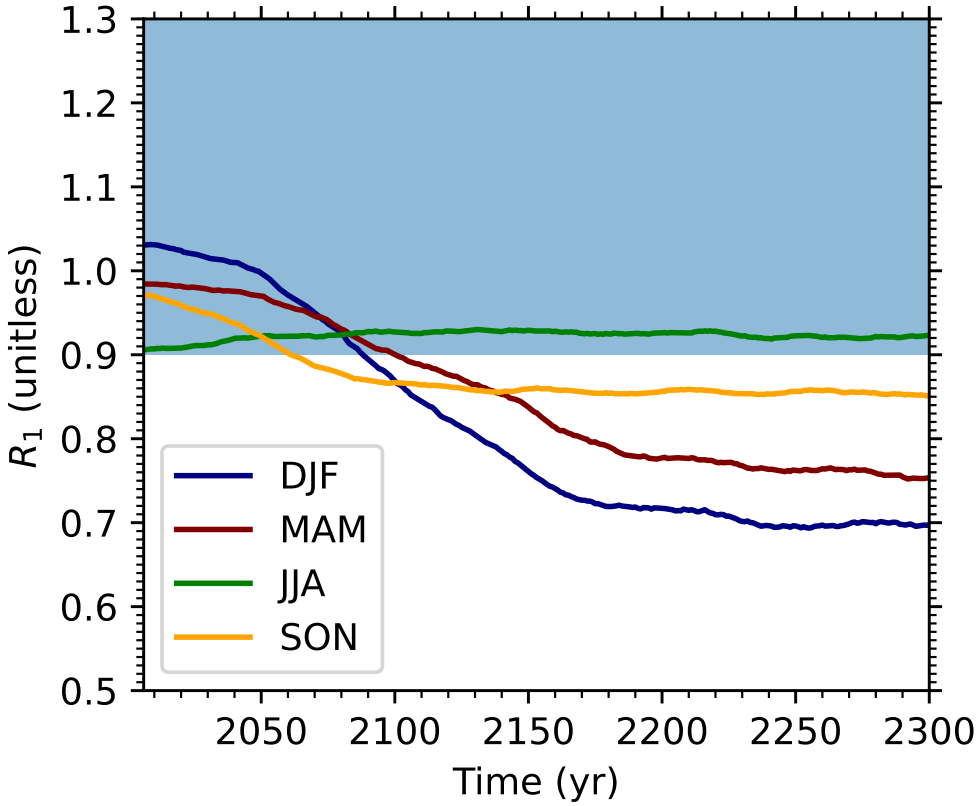

Figure S20. The CMIP5 Arctic energy balance regime response during winter (DJF), spring (MAM), summer (JJA), and fall (SON). Blue and white regions indicate RAE and RCAE, respectively.

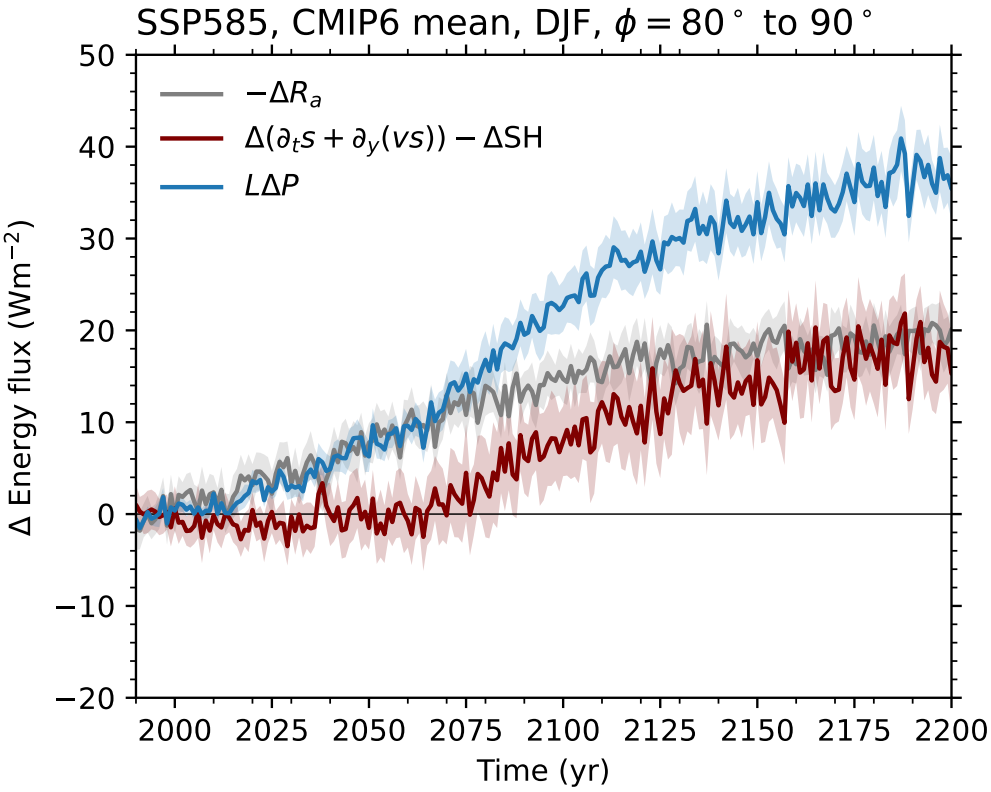

Figure S21. The wintertime (DJF) dry static energy (DSE) energy budget decomposed into atmospheric radiative cooling (gray line), latent heat released from precipitation (blue line), and atmospheric DSE flux convergence plus storage minus surface sensible heat flux (maroon line) for the CMIP6 multimodel mean of the extended SSP585 run. The shading indicates the 5–95% confidence interval.

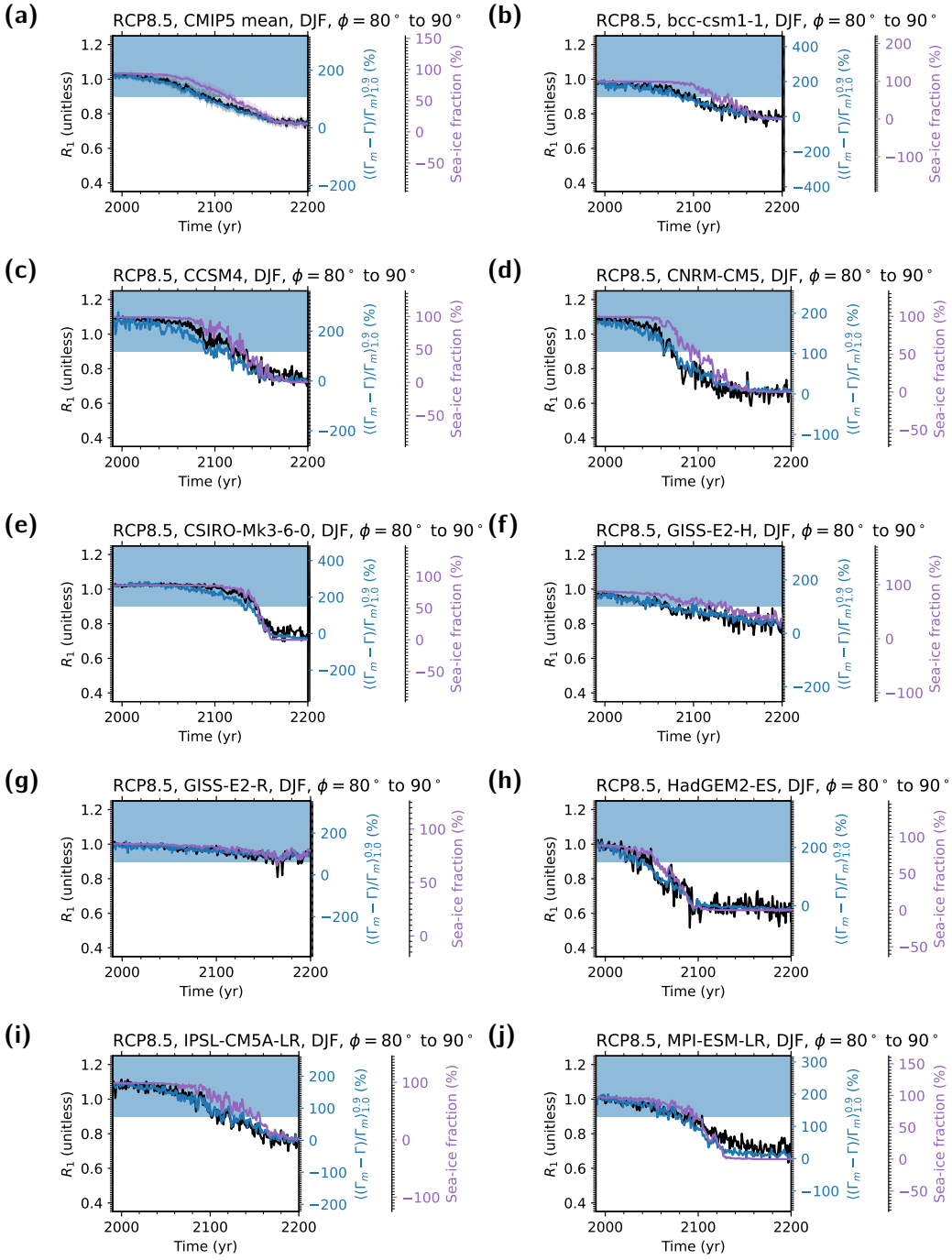

Figure S22. Same as Fig. 1a but (a) for the CMIP5 multimodel mean and (b–j) individual CMIP5 models.

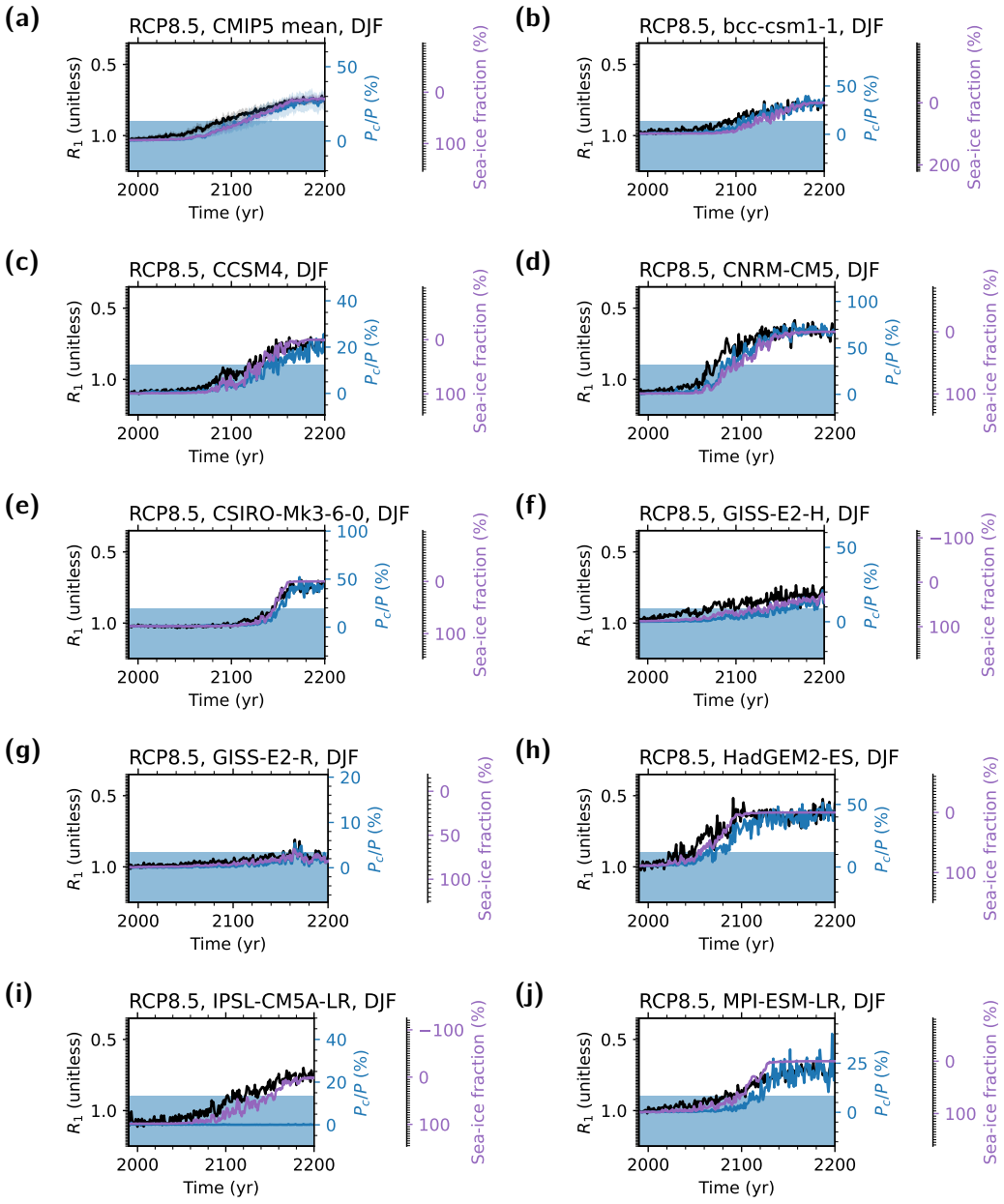

Figure S23. Same as Fig. 1b but (a) for the CMIP5 multimodel mean and (b–j) individual CMIP5 models.

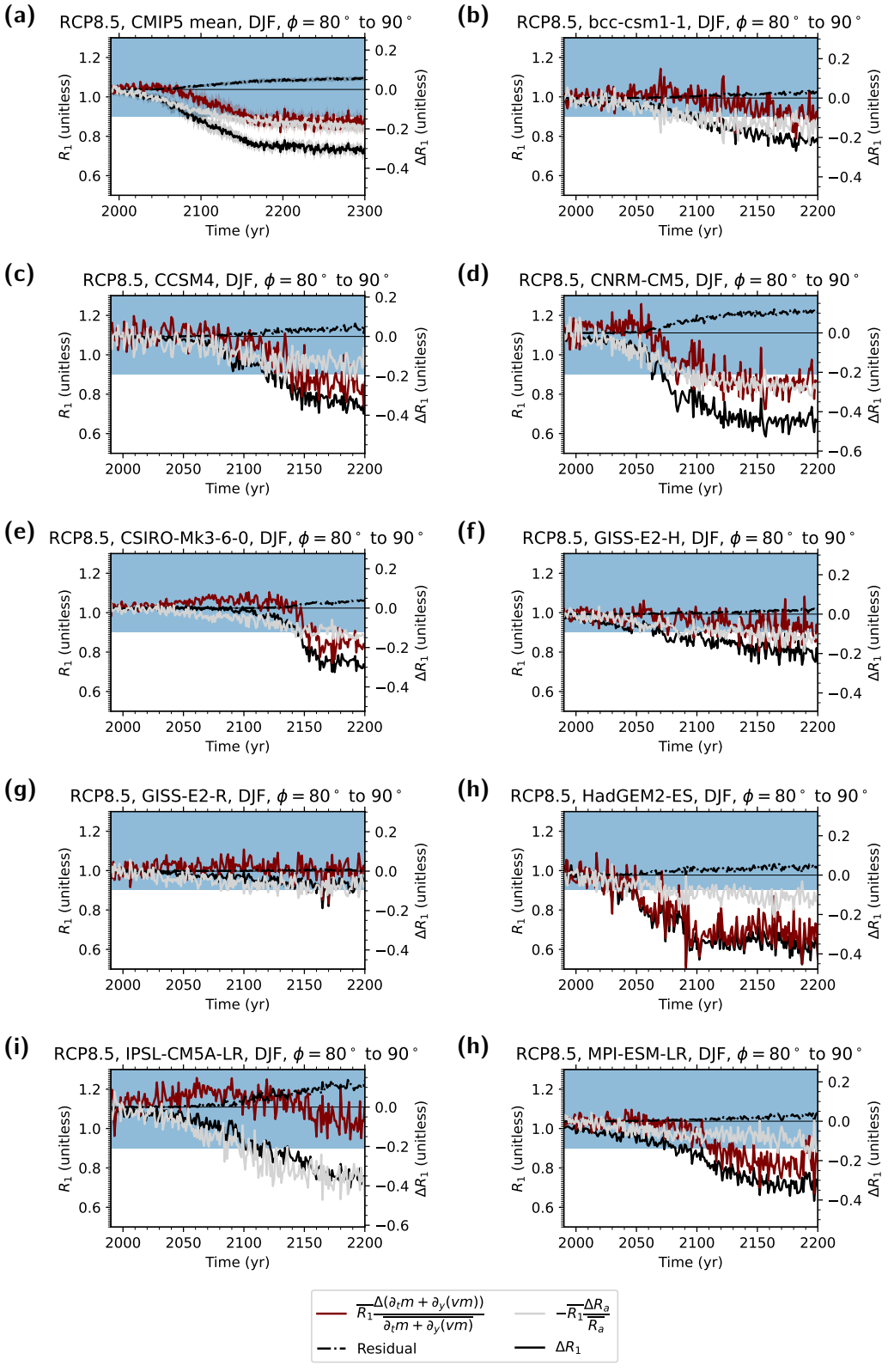

Figure S24. (a) Same as Fig. 2 but (b–h) for individual CMIP5 models.

Figure S25. Same as Fig. 2 but (a) for the CMIP5 multimodel mean and (b–j) individual CMIP5 models.

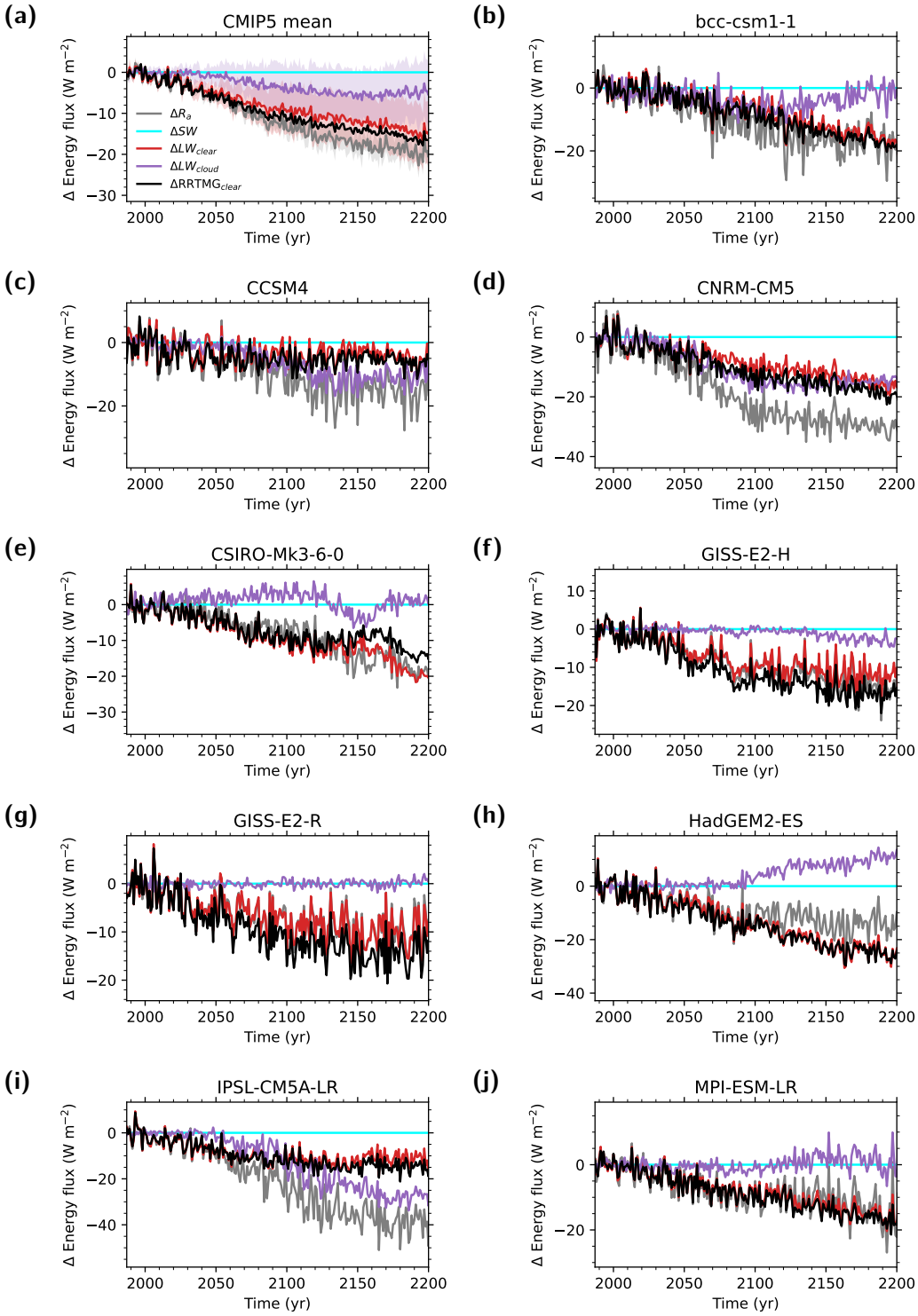

Figure S26. Same as Fig. 3a but (a) for the CMIP5 multimodel mean and (b–j) individual CMIP5 models.

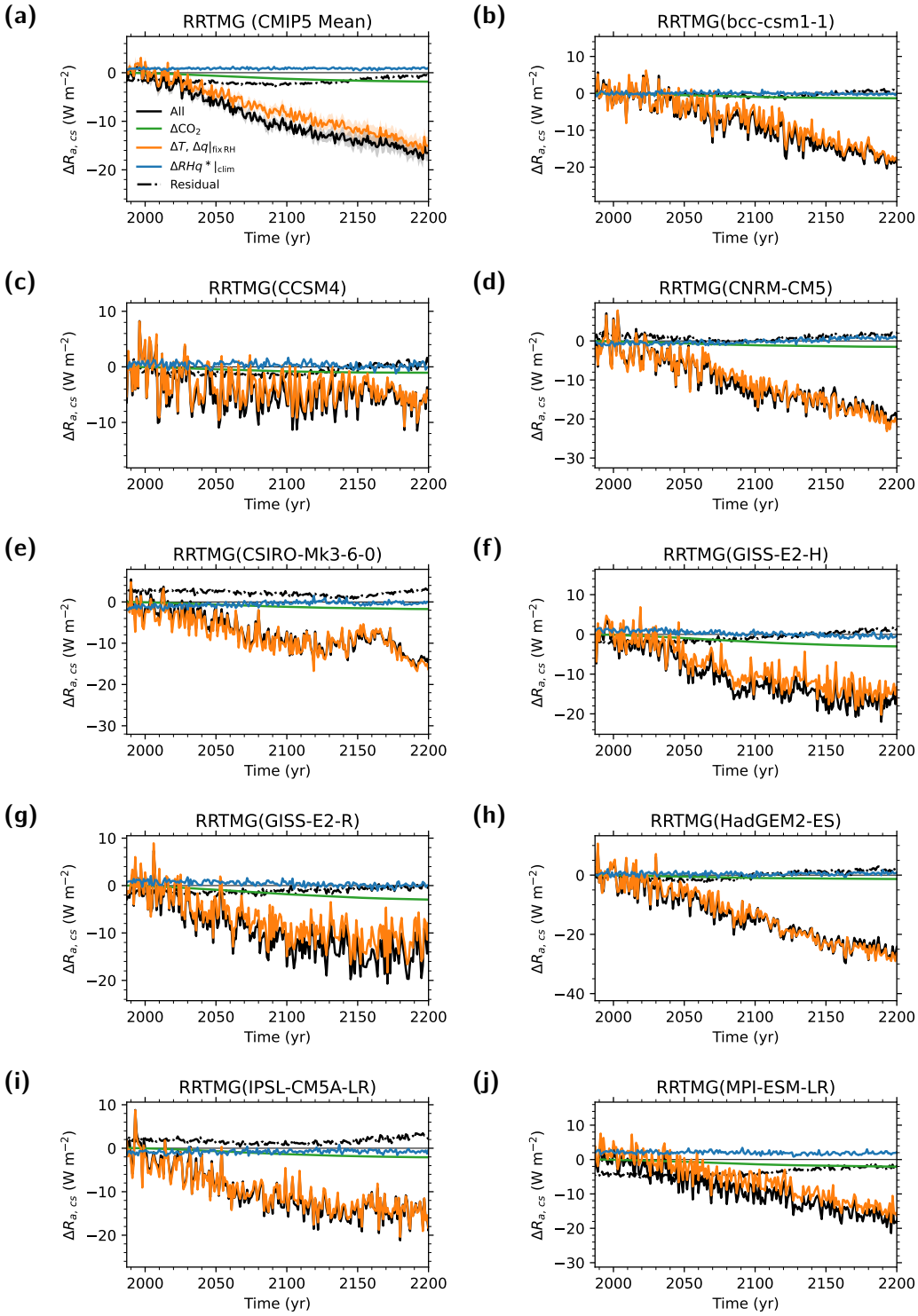

Figure S27. Same as Fig. 3b but (a) for the CMIP5 multimodel mean and (b–j) individual CMIP5 models.

References

Winton, M. (2005). Simple Optical Models for Diagnosing Surface–Atmosphere Shortwave Interactions. *Journal of Climate*, *18*(18), 3796–3805. doi: 10.1175/JCLI3502.1